A game theory-inspired algorithm for automating the design of non-periodic integral 3D woven composite preforms without scale limitations using a manufacturing-based parameterization

Zhen-Pei Wang[a*], Brian N. Cox[b], Shemuel Joash S/O Kuehsamy[a], Mark Hyunpong Jhon[a], Olivier Sudre[c], N. Sridhar[a], Gareth Conduit[d]

[a]*Institute of High Performance Computing (IHPC), Agency for Science, Technology and Research (A*STAR), 1 Fusionopolis Way, #16-16 Connexis, Singapore 138632, Republic of Singapore.*

[b]*Sherman Oaks, CA, USA*

[c]*Pratt & Whitney, USA*

[d]*The Studio, Chesterton Mill, Cambridge, United Kingdom, UK; and Theory of Condensed Matter, Department of Physics, University of Cambridge, J. J. Thomson Avenue, Cambridge, CB3 0HE, UK*

Abstract

Three-dimensional non-periodic woven composite preforms have sufficient design flexibility that tows can be aligned along principal loading paths even in shaped structural components with detailed local features. While this promises competitive performance, the feasible design space is combinatorically large, far beyond exhaustive search. Inspired by multi-agent game theory, here we propose a generative design method called the Background Vector Method (BVM) which treats weaving tows as different agents finding their best matching background vectors derived from different design requirements. The BVM can generate designs that are tunable to a specific balance of requirements by adjusting scalar weights, concurrently accounts for local and global architecture, utilizes a manufacturing-based parameterization that assures fabricability, and is highly computationally efficient. The scope of possible designs is illustrated by re-creating common periodic 3D weaving patterns and novel complex non-periodic architectures. The BVM also offers a simple design pathway to creating preforms with cavities, ducts, and other open volumes.

Keywords

3D woven/textile composite, Combinatorial Design optimization, Integral design, Virtual specimen

* Corresponding author
Email address: wangzp@ihpc.a-star.edu.sg (Zhen-Pei Wang)

1. Introduction

3D woven composites have several potential advantages over conventional 2D woven preforms. Interlocking woven tow structures ensure good damage tolerance [1-16], which reduces delamination failure in impact events such as bird strikes. Non-periodic integrally woven designs [17-20] can achieve near-net-shape structures, making it possible to fabricate 3D composite structures with complex geometries without requiring subsequent machining to conform to the external shape or form internal holes and cavities [21]. Finally, a tailored 3D tow structure can reinforce against local load variations without adding weight [7,17].

However, the combinatorial optimization of an unrestricted 3D tow architecture, where tow topology is characterized by typically 10^3 -10^6 distinct candidate tow orderings per mm^2 of fabric, poses formidable computational challenges. Shying away from such complexity, current design methodologies are often limited to assembling small unit cells of simplified architecture or applying other restrictions that negate generality in design outcomes. One proposed strategy is to evaluate and choose from standard periodic designs based on generalized requirements [22]. Another is to use heuristic algorithms, e.g., genetic algorithms, to optimize one periodic unit cell [23-27], but without optimizing the overall structure. Geometry design modelling [21, 28-32] or topology optimization techniques [33] have been used with restrictions that reduce the design difficulty but tend to limit applicability.

Some approaches couple fully periodic or other simplified local structures with homogenization for use in a multiscale model [34, 35]. But homogenization makes it difficult to design manufacturable structures, as the local weave design in two-scale designs is not explicit. Some of the most complex textile designs have been derived by experience, intuition, and a combination of elementary analysis and testing of local stress conditions in tow-scale sub-elements [17-20, 36]. However, none of these designs was formally optimized, nor can the intuitive methods that were used be easily replicated for other complex design challenges.

Using concepts similar to multi-agent game theory, we propose a generative methodology called the Background Vector Method (BVM) that designs non-periodic 3D weave architectures concurrently at all scales. The method treats different weaving tows as different agents, with a design parameterization that ensures the designs are manufacturable (e.g., Cox et al. [18,31]). The BVM introduces a set of background

vector fields that are defined by the local mechanical requirements of various component-scale performance goals. A deterministic but tuneable algorithm generates different tow configurations based on the weighting of the background vector fields: tow designs thus balance competing requirements.

The BVM echoes prior design approaches for composites that seek to match local fibre orientation to local load paths, both in human designs [37] and in evolution (e.g., the structure of trabecular bone [38] and other bio-structures suggestive of Wolff's law [39]) but does so while respecting the unique topological constraints of 3D weaving. By concurrently accounting for part-scale and tow-scale design requirements, the BVM enables the design of parts with generally complex geometry, which might substantially broaden the applicability of 3D integral woven composites.

2. A manufacturing-based design parameterization of non-periodic woven tow architecture

This study focuses on non-periodic woven tow architectures that can be fabricated on an "orthogonal loom" in the paradigm of Fig. 1. In the fabrication process, there are two sets of orthogonal tows: the weft tows and the warp tows. The warp tows are organized into "warp stacks" aligned parallel to the x-axis and spaced out along the y-direction with a gap of δ_{warp}, while the weft tows are organized into "weft stacks" aligned parallel to the y-axis and spaced out along the x-direction with a gap of δ_{weft}. Tows within a warp or weft stack are distributed vertically in the orientation of Fig. 1, warp stacks occupying z-x planes and weft stacks z-y planes.

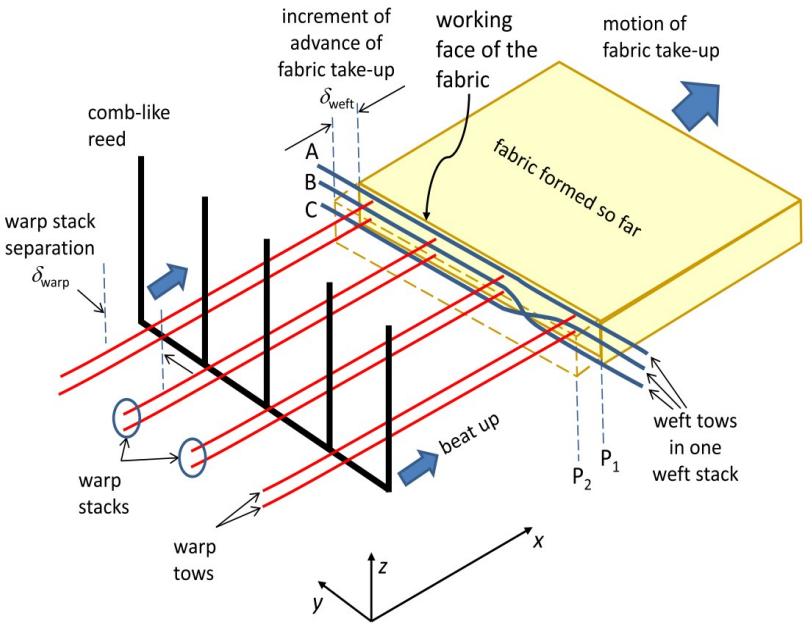

Figure 1. Schematic of the manufacture of a 3D woven composite preform using a Dobby or Jacquard-head loom [18].

The coordinate system $\{x, y, z\}$ of Fig. 1 will be associated throughout this article with the indices $\{i, j, k\}$. Since different warp tows are distinguished by their discretized y-coordinates, warp stacks will be tagged by the index j; and weft stacks, being distinguished by their discretized x-coordinates, will be tagged by the index i. The index k or sometimes will be used to label the z-coordinates of points on a 3D grid.

During the weaving process, weft tows are sequentially woven through the warp stacks. The structure is determined by the locations at which the weft tow enters a particular warp stack (how many warp tows are above or below that location) through re-positioning of heddles holding the warp tows. Any weave architecture can be uniquely distinguished by topological ordering rules that specify the arrangement of warp and weft within any intersection of warp and weft stacks (e.g., Cox et al. [18]).

Using this parameterization, the structure of 3D non-periodic woven composites can be described in a way that can be translated easily to machine operations for manufacturing. Topological-ordering parameterization mirrors the manufacturing process: an assignment of the ordering integer

$$\zeta_{i,p}^{(j)} = q \qquad (1)$$

specifies that, at the intersection of the j^{th} warp stack and the i^{th} weft stack, the p^{th} weft tow is to be passed

by the loom above a number q of the warp tows in the warp stack. The design of a single weft stack i is described by the array of elements $\zeta_{i,p}^{(j)}$ for all j and p (Table 1). If there are no limits placed on $\zeta_{i,p}^{(j)}$, then more than one weft tow from the same stack might be assigned the same ordering position at an intersection, in which case "secondary ordering rules" specified in [18] resolve ambiguity.

Warp tows within any stack are often assumed to be fixed in their mutual ordering in applying Eq. (1). But this restriction can be relaxed by allowing "warp switching" in the actions of the weaving loom [18].

Table 1 The locations of the weft tows p in weft stack i at intersections with different warp stacks j as specified by topological ordering rules.

Weft tow (*i, p*)		Weft tow location						
		…	$i,1$	$i,2$	$i,3$	$i,4$	$i,5$	…
Warp stack j	1	…	$\zeta_{i,1}^{(1)}$	$\zeta_{i,2}^{(1)}$	$\zeta_{i,3}^{(1)}$	$\zeta_{i,4}^{(1)}$	$\zeta_{i,5}^{(1)}$	…
	2	…	$\zeta_{i,1}^{(2)}$	$\zeta_{i,2}^{(2)}$	$\zeta_{i,3}^{(2)}$	$\zeta_{i,4}^{(2)}$	$\zeta_{i,5}^{(2)}$	…
	3	…	$\zeta_{i,1}^{(3)}$	$\zeta_{i,2}^{(3)}$	$\zeta_{i,3}^{(3)}$	$\zeta_{i,4}^{(3)}$	$\zeta_{i,5}^{(3)}$	…
	4	…	$\zeta_{i,1}^{(4)}$	$\zeta_{i,2}^{(4)}$	$\zeta_{i,3}^{(4)}$	$\zeta_{i,4}^{(4)}$	$\zeta_{i,5}^{(4)}$	…
	…	…	…	…	…	…	…	…

Table 1 formally links the present work to that of [18]. In [18], the set of all $\zeta_{i,p}^{(j)}$ served as initial conditions: they were translated into pair-wise topological ordering rules via which a 3D model of a pre-conceived textile defined by the $\zeta_{i,p}^{(j)}$ could be expediently generated. In [18], the table of all $\zeta_{i,p}^{(j)}$ was built by hand, a tedious process that requires high expertise, since the builder must already have the 3D textile in mind and must foresee the path from the $\zeta_{i,p}^{(j)}$ to that textile. The present work generates information equivalent to the $\zeta_{i,p}^{(j)}$ automatically, guided not by a pre-conception of the 3D textile but by functional design objectives, and the BVM may therefore be operated by someone with modest textile expertise. The present work proceeds by a different path to generate 3D models of textiles, demonstrating many but not yet all the features that can be supported by the very flexible design algorithm of [18].

3. Challenges in the design of woven composites

3.1 Design Considerations

Designing 3D integral woven composites requires balancing competing structural requirements in selecting tow orientations and positions. Objectives include:

- Providing an acceptable compromise between in-plane properties, for which tows should be oriented in the plane of the fabric, and delamination resistance and interlaminar shear strength, for which tows should traverse through the fabric.
- Varying the selected architecture from one region to another of a component to match the generally complex loading configuration that the component must support. Typically, the optimal architecture may exhibit periodicity in some regions and be non-periodic elsewhere; and must transition between periodic and non-periodic regions in such a way that no manufacturing difficulty or mechanical weakness is associated with the transition.
- Enabling the possibility of vacant volumes in a structure (cavities, ducts, etc.).

3.2 The 2D and 3D design problems for arbitrary, non-periodic tow architecture

Any 3D woven fabric created by a loom of the type of Fig. 1 can be regarded as an orthogonal array of 2D warp and weft sections (z-x and y-z planes, respectively, in Fig. 1), each section comprising a single stack of warp or weft tows. The 2D sections intersect one another at a rectangular grid of points in the x-y plane. The intersection $o_{i,j}$ of warp stack j with weft stack i contains $n_{warp}^{(j)}+n_{weft}^{(i)}$ tows in total, stacked vertically in the orientation of Fig. 1. Throughout this paper, all warp and weft tows are assumed to have equal thickness h in the z-direction (this assumption is easily relaxed in a developed code), so that the warp and weft tows at any intersection occupy sites with z-coordinates

$$z_{ij}^{(k)}=kh,\ k=1,\ldots,n_{warp}^{(j)}+n_{weft}^{(i)}. \tag{1a}$$

The mix of $n_{warp}^{(j)}+n_{weft}^{(i)}$ tows fall into one of the sets O of all possible orderings of the warp and weft tows in the z-direction, i.e., all possible assignments of specific warp and weft tows to z-positions $h, 2h, 3h, \ldots$. A single design of the architecture is the set of chosen orderings

$$O_d=\left\{O_{i,j}\middle|i=1,\ldots,N_{weft};\ j=1,\ldots,N_{warp}\right\} \tag{1b}$$

for all intersections $o_{i,j}$. Choosing O_d is the fundamental topological design problem. The total number of distinct orderings $O_{i,j}$ possible for intersection $o_{i,j}$ for distinguishable warp and weft tows is

$$n_O^{(ij)} = \left(n_{warp}^{(j)} + n_{weft}^{(i)}\right)! \quad . \tag{2a}$$

Since orderings at all intersections can legally be made independently of each other (in terms of the laws of operation of a weaving loom in which warp switches are permitted [18]), the number of distinct orderings, i.e., the size of the design space O_d, in a textile with $N = N_{warp} N_{weft}$ intersections is

$$N_{max}^{(design)} = \left(n_O^{(ij)}\right)^N. \tag{2b}$$

Design optimization by exhaustive search will always remain infeasible. However, if a design methodology can be formulated that addresses the environment of each intersection independently of the design problem for all other intersections, then the size of the design space to be considered at any step is capped by the number of different orderings at a single intersection, which is relatively modest.

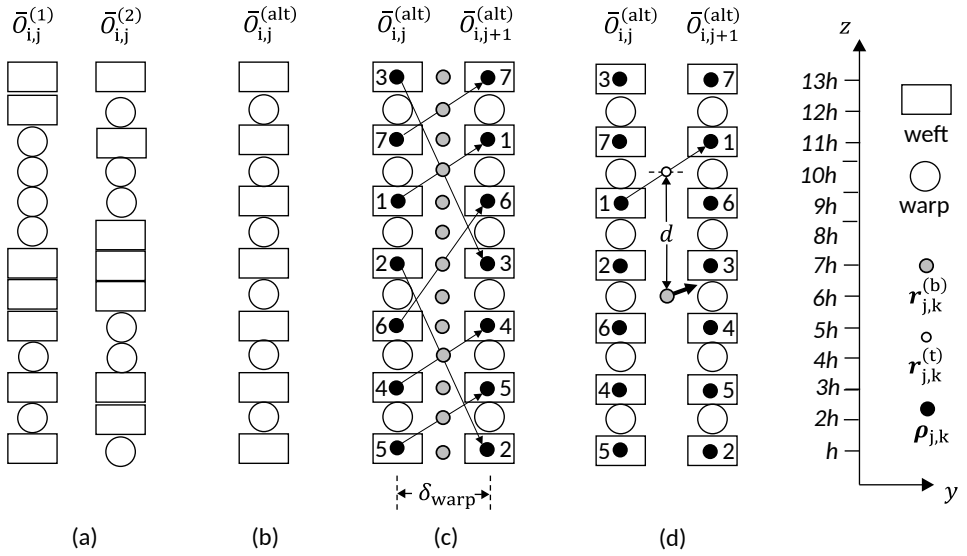

Figure 2. (a) Two examples of orderings $\overline{O}_{i,j}$ of indistinguishable warp and indistinguishable weft tows at intersection $o_{i,j}$. (b) The specific ordering $\overline{O}_{i,j}^{(alt)}$ in which indistinguishable weft alternate with indistinguishable warp. (c) Instantiations of the restricted orderings $\overline{O}_{i,j}^{(alt)}$ and $\overline{O}_{i,j+1}^{(alt)}$ at successive intersections within a weft section, with now distinguishable weft tows numbered and arrows indicating tow locus vectors originating at the locations $\rho_{j,k}$ (black circles) that are allowed for weft tows. The tow locus vectors are instantiations of the tow-path vector field. (d) A background vector (thick arrow), its reference point $r_{j,k}^{(b)}$ (gray circle), and its distance d from a tow-path reference point $r_{j,k}^{(t)}$ (small open circle). With $n_{warp} = 6$ and $n_{weft} = 7$.

3.3 Designs with restricted orderings

Fortunately, it is possible to reduce the allowed design space to a manageable size while retaining sufficient generality to support desirable outcomes.

- Consider the set $\overline{O}$ of orderings available to any intersection $o_{i,j}$ that are defined by whether sites $k=1,\ldots,n_{warp}^{(j)}+n_{weft}^{(i)}$ are occupied by warp or weft tows, without distinguishing warp tows from each other or weft tows from each other (Fig. 2a). Restricting allowed choices from $O_{i,j}$ to those consistent with a single choice $\overline{O}_{ij}$ of $\overline{O}$ for intersection $o_{i,j}$, there are

$$\overline{n}_O^{(ij)}=\frac{\left(n_{warp}^{(j)}+n_{weft}^{(i)}\right)!}{n_{warp}^{(j)}!\,n_{weft}^{(i)}!} \tag{2c}$$

  possible remaining orderings, still large but much less than $n_O^{(ij)}$.

- Given a fixed $\overline{O}_{i,j}$ at intersection $o_{i,j}$, the design spaces for warp and weft become separated: the restriction of orderings enforces the warp tows to be assigned to a fixed subset $\left\{\overline{z}_{ij}^{(k)},k=1,\ldots,n_{weft}^{(i)}\right\}$ of the z-positions of Eq. (1a) and the weft tows to the complementary subset. Re-arranging the warp tows has no effect on the positional assignments available to weft tows, and vice versa. The number of distinct ways of ordering the $n_{warp}^{(j)}$ warp tows and $n_{weft}^{(i)}$ weft tows in their allowed positions are, respectively,

$$\overline{n}_O^{(ij,weft)}=n_{weft}^{(i)}!;\ \overline{n}_O^{(ij,warp)}=n_{warp}^{(j)}! \tag{2d}$$

- Last, consider the entire 2D section defined by the single weft stack i (a y-z plane in Fig. 1). If the orderings at all intersections in this 2D section are fixed to some instantiation of $\overline{O}$, then the design space of the weft tows in section i becomes independent of the design space for any other section, whether warp (z-x plane orthogonal to weft stack i) or weft (y-z plane parallel to weft stack i). This is equally true if one considers the 2D section defined by a single warp stack.

Given the preceding, the special case to be studied in this article is chosen, wherein the ordering at each intersection $o_{i,j}$ appearing in the entire structure is restricted to a single common instantiation $\overline{O}_{i,j}$ of $\overline{O}$ and the design spaces of all 2D sections in the entire structure, whether warp or weft, are independent of each other. That is, the design space for an entire 3D structure devolves into a set of mutually independent

design spaces for the 2D sections.

In the BVM, this independence of the design spaces for different sections is exploited by an algorithm applicable to one 2D section at a time. The manner in which this design constraint might be relaxed advantageously (mutual dependence admitted among designs of different 2D sections) without undue design space expansion is specified in Sect. 6.

Finally, acting within the design space of a single section, the BVM reduces the problem size as far as is physically permissible by presenting an algorithm that can be executed sequentially through the 2D section, one intersection at a time.

4. Background Vector Method

4.1 Method Overview

The physical concept of the BVM is to let the tows (game agents) in any 2D section pair with "background vectors", which present a variety of local architectural options that are likely to support different possible local stress states in an efficient manner. Any background vector represents a local target direction for a segment of a tow locus during design, with the strength of its influence proportional to the vector's magnitude. Two classes of background vectors, termed bespoke background vectors and genetic background vectors, respectively, are introduced.

4.2 Exemplification for a 2D weft section

The number of intersections in a 2D weft section equals the total number of warp stacks, set in all examples to $N_{warp}=36$. The number of warp tows in any warp stack is set to be uniformly $n_{warp}=6$. The number of weft tows in any weft stack is set to be uniformly either $n_{weft}=7$ or $n_{weft}=12$.

A single weft section is taken as the study case. The notational simplification is used in this section that the weft index i can therefore be omitted. The restricted set of orderings $\overline{O}_j$ allowed at any intersection o_j with warp stack j is set to either the "alternating" pattern $\overline{O}^{(alt)}=\{weft, warp, weft, \ldots, weft, warp, weft\}$ if $n_{weft}=7$ (Fig. 2b) or the "{1,2}" pattern $\overline{O}^{(1,2)}=\{weft, warp, weft, weft, warp, \ldots, warp, weft, weft, warp, weft\}$ if $n_{weft}=12$. The design task for the weft tows in a 2D weft section is to allocate the 7 or 12 weft tows to the z-coordinates allowed for the centers of mass of weft tows at intersection o_j (Fig. 2c). Given $\overline{O}^{(alt)}$ or $\overline{O}^{(1,2)}$ at

intersection o_j and tows of uniform thickness h, the allowed z-coordinates are $z = kh$ where $k \in \overline{\Omega}$, an integer set of allowed location indices:

$$\overline{\Omega} \equiv \begin{cases} \{1,3,5,7,9,11,13\} & \left(n_{weft} = 7; \overline{O} = \overline{O}^{(alt)}\right) \\ \{1,3,4,6,7,9,10,12,13,15,16,18\} & \left(n_{weft} = 12; \overline{O} = \overline{O}^{(1,2)}\right) \end{cases} \tag{3a}$$

The total number of available locations for weft tows at any intersection is n_{weft}. The total thickness of the textile fabric, measured in terms of the centers of mass of tows, is represented by

$$H = \begin{cases} 12h & \left(n_{weft} = 7; \overline{O} = \overline{O}^{(alt)}\right) \\ 17h & \left(n_{weft} = 12; \overline{O} = \overline{O}^{(1,2)}\right) \end{cases}. \tag{3b}$$

In addition to the location indices $\overline{\Omega}$, the complementary location indices

$$\acute{\Omega} = \begin{cases} \{2,4,6,8,10,12\} & \left(n_{weft} = 7; \overline{O} = \overline{O}^{(alt)}\right) \\ \{2,5,8,11,14,17\} & \left(n_{weft} = 12; \overline{O} = \overline{O}^{(1,2)}\right) \end{cases} \tag{3c}$$

will be used in defining background vectors.

4.3 Bespoke background vectors

Bespoke background vectors (denoted b) represent load-paths arising in the subject component when it experiences the specific boundary or body forces expected in service. Multiple sets of bespoke background vectors might be included for multiple service loading cases. Load paths can be derived from fields of principal stresses found via a Finite Element Method (FEM) simulation. The simulation can be executed using a homogenized material model. In iterative design, it may be advantageous to re-determine load paths by analysing a heterogeneous material model built from the current generated textile architecture (Sect. 6).

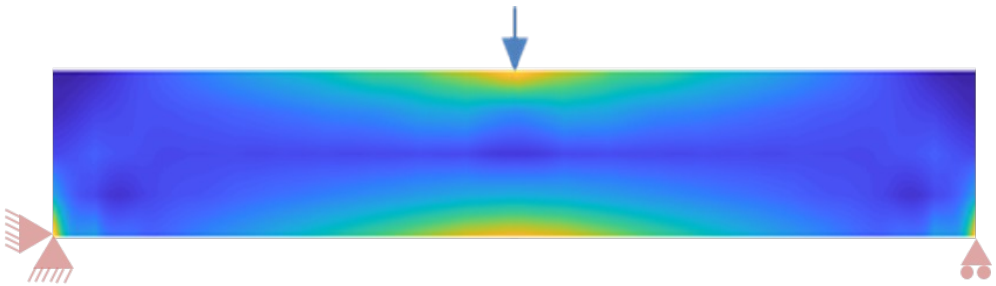

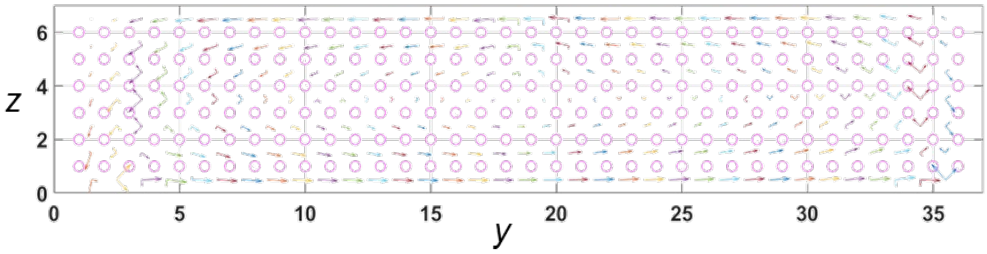

Figure 3. Upper: von Mises stress in a simply supported beam in plane strain. Lower: derived principal stresses evaluated at reference points.

Fig. 3 illustrates the derivation of bespoke background vectors for a component loaded in three-point bending. In this figure, circles are the locations of warp tows, between which weft tows (which are not shown) must pass. The principal components of the 2D stress field (in an anisotropic 3D case, the principal components of the 2D stress field found in the plane of the 2D section by rotational transformation of a 3D stress field) are recorded as the pair $\sigma_{j,k} \equiv \left\{ \sigma_{j,k}^{(1)}, \sigma_{j,k}^{(2)} \right\}$ at each of an array of "background reference points" $r_{j,k}^{(b)}$ (Fig. 2). The reference points lie mid-way between successive intersections o_j and o_{j+1} and are distributed through the thickness of the design domain (y, z):

$$r_{j,k}^{(b)} = \left[\left(j - 1 + \frac{1}{2} \right) \delta_{warp}, kh \right]^T, (j = 1, \ldots, N_{warp} - 1 \text{¿} \tag{4a}$$

with $k \in \overline{\Omega}$ and δw_{warp} the intersection spacing (Fig. 2).

The principal stress vectors for all reference points constitute a bespoke background vector set

$$B_L = \left\{ b_{j,k} \middle| j = 1, \ldots, N_{warp} - 1; k \in \overline{\Omega} \right\} \tag{4b}$$

where $b_{j,k} = \frac{1}{\sigma_{max}} \sigma_{j,k}$, with $\sigma_{max} = \max_{r,j,k} \sigma_{j,k}^{(r)}$. The normalization $1/\sigma_{max}$ ensures that the background vectors are dimensionless quantities whose magnitude is bounded by unity.

4.4 Generic background vectors

Generic background vectors (denoted g) represent load-paths that would arise if the component experienced a simple generic loading condition: uniform in-plane tension/compression, uniform through-thickness tension/compression, pure bending, uniform shear, etc. Background vectors for generic loads are defined by simple formulae indicative of load paths obtained by closed-form analysis. They are exemplified here by four instances, defined by the following formulae and illustrated in Fig. 4.

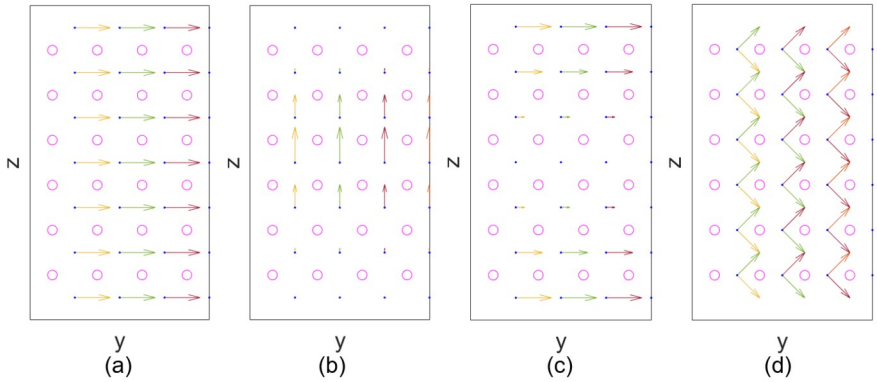

Figure 4. Generic background vectors suggested by (a) in-plane tension/compression; (b) through-thickness tension/compression; (c) pure bending; (d) interlaminar shear.

Uniform in-plane tension/compression:

$$b_{j,k}^{(t)}=\left[1,0\right]^{T} \tag{5a}$$

Through-thickness loading:

$$b_{j,k}^{(z)}=\left[0,\cos^{3}\left(\frac{-\pi}{2}+\frac{(k-1)h\pi}{t-h}\right)\right]^{\mathrm{T}} \tag{5b}$$

Bending:

$$b_{j,k}^{(b)}=\left[\cos^{2}\left(\frac{(\varphi_k-1)h\pi}{t-h}\right),0\right]^{\mathrm{T}} \tag{5c}$$

Uniform through-thickness shear:

$$b_{j,k}^{(s1)}=\left[\sqrt{2}/2,\sqrt{2}/2\right]^{\mathrm{T}};\ b_{j,k}^{(s2)}=\left[\sqrt{2}/2,-\sqrt{2}/2\right]^{\mathrm{T}} \tag{5d}$$

where the reference point in each case is $r_{j,k}^{(b)}$ of Eq. (4a), with $k\in\overline{\Omega}$ (Eqs. (5a-5c)) or $k\in\acute{\Omega}$ (Eqs. (5d)).

The examples of Eq. (5) are all invariant in the y-direction (along the subject 2D weft section), but some vary in the z-direction (through the thickness). Notwithstanding the invariance in the y-direction, including an intersection label j in notation allows compactness in writing certain expressions below. Each of the background vectors of Eq. (5) can be gathered into a generic background vector array:

$$B_g=\left\{b_{j,k}^{(g)}\middle|\, j=1,\ldots,N_{warp}-1;k\in\overline{\Omega}\cup\acute{\Omega}\right\},\ g\in\left\{t,z,b,s\right\} \tag{6}$$

with $s\equiv\left\{s1,s2\right\}$.

4.5 Total background vector field

All bespoke and generic background vector fields are collected into a single total background vector

field: $B = B_L \cup B_g = B_L \cup B_t \cup B_z \cup B_b \cup B_s$, or, in a simplified form,

$$B = \left\{ B_m \; \forall \; m \in \{ L, t, z, b, s \} \right\}. \tag{7}$$

The total background vector field may be regarded as a (non-orthonormal) basis function set for the expression of candidate local weave architectures. Candidate tow paths are formed not as linear combinations of the basis functions, but via a nonlinear sorting algorithm (see below); and tow path segments are defined not on a continuous space but on the integer space that defines the allowed topology of the woven structure. Nevertheless, as with any basis function set, the background vector field is amenable to expansion to higher orders (finer details enabled in local architectures by expansion of the total background vector field to include further bespoke or generic cases) and such expansion can be tested for convergence of its influence on the objective functions of an optimization procedure.

4.6 Candidate and selected tow-path vectors

Candidate tow-path segments between successive intersections in a 2D section also constitute a set of vectors, denoted t (e.g., Fig. 2c). In the paradigm of a 2D weft section, a candidate segment passes from z-coordinate kh at intersection o_j to z-coordinate $k\,h$ at intersection o_{j+1}. A normalized candidate tow-path vector is written

$$t_{j,k,k} = \frac{1}{\left\| \left[\delta w_{warp}, k\,h - kh \right] \right\|} \left[\delta w_{warp}, k\,h - kh \right]^{\mathrm{T}} \quad (k \in \overline{\Omega}, k \in \overline{\Omega}) \tag{8a}$$

The tow-path vector originates at location $\rho_{j,k} = ¿¿$ $(k \in \overline{\Omega})$ within intersection o_j and is associated with a "tow-path reference point" $r_{j,k}^{(t)} = \rho_{j,k} + \frac{1}{2} t_{j,k,k} (j = 1, \ldots, N_{warp} - 1 ¿$ (Fig. 2), which is the centre point of the tow segment. The candidate tow-path vectors form a vector array:

$$T = \{ t_{j,k,k} \vee k \in \overline{\Omega}; k \in \overline{\Omega}; j = 1, \ldots, N_{warp} - 1 \} \tag{8b}$$

Candidate tow-path vectors that are selected form a concatenated continuous tow path, which is recorded as a vector τ_w comprising the z-coordinate indices that weft tow w passes through at each intersection

$$\tau_w = \left\{ \tau_j^{(w)} \middle| \, j = 1, \ldots, N_{warp} \right\} \tag{8c}$$

with $\tau_j^{(w)} \in \overline{\Omega}$.

4.7 Reinforcing Performance Index

The potential utility of candidate tow-path vectors is evaluated in terms of the degree to which they match the different members of the total load-path background vector set. A "reinforcing performance index" $P[j;m,;k,k]$ measures how well a candidate tow-path segment aligns with any one background vector:

$$P[j;m,;k,k]=c_m f[H-d]\left|t_{j,k,k}\cdot b_{j,}^{(m)}\right|+\epsilon[j,k], \text{ with } d\equiv\left|r_{j,k}^{(t)}-r_{j,k}^{(b)}\right| \tag{9a}$$

where $t_{j,k,k}$ is a candidate tow-path segment originating at $\rho_{j,k}$ in o_j with $k\in\overline{\Omega},k\in\overline{\Omega}$; $b_{j,}^{(m)}$ is a background vector of type $m\in\{L,t,z,b,s\}$ associated with reference point $r_{j,}^{(b)}$ between intersections o_j and o_{j+1} with $\in\overline{\Omega}$ if $m\in\{L,t,z,b\}$ and $\in\acute{\Omega}$ if $m\in\{s\}$; c_m is an undetermined weighting factor (see Sect. 4.8); H is the total thickness of the textile at intersection o_j; d is the distance between the tow-path and background reference points (Fig. 2d); and $\epsilon[j,k]$is a history term. The weight c_m for $m\in s\equiv\{s1,s2\}$ is defined to be the same for $s1$ and $s2$.

The functions $f[H-d]$ and $\epsilon[j,k]$ are available for choice. Choosing $f[H-d]=\frac{H-d}{H}$ allocates higher influence if d is small. Choosing

$$\epsilon[j,k]=\alpha\left|t_{j,k,k}\cdot t_{j-1,\tau_{j-1}^{(w)},k}\right|_{j>1}+\beta\left|t_{j-1,\tau_{j-1}^{(w)},k}\cdot t_{j-2,\tau_{j-1}^{(w)},k}\right|_{j>2} \tag{9b}$$

where $\tau_{j-1}^{(w)}$ and $\tau_{j-2}^{(w)}$ are elements of the already-determined tow-path record τ_w for weft tow w up to intersection o_j, with w the tow occupying location k and $\alpha,\beta\ll 1$ two constants, helps disambiguate cases where the same $P[j;m,;k,k]$ arises for different combinations of candidate tow-path vectors and background vectors.

4.8 Sequential parametric design strategy

All weft tows w are assigned locations in the first intersection o_1, thus establishing $\tau_1^{(w)}$, the first element of the tow-path record τ_w for each tow. Selection of tow-path segments between intersections o_j and o_{j+1} ensues as follows.

a. All background vectors tagged to reference points $r_{j,}^{(b)}$ are collected into a set

$$B^{(j)}=\left\{b_{j,}^{(m)}\middle|m\in\{L,t,z,b,s\},\in\overline{\Omega}\vee\in\acute{\Omega}\right\}.$$

b. All candidate tow-path vectors tagged to origin points $o_{j,k}$ are collected into a set

$T^{(j)}=\left\{t_{j,k,k}\middle|k\in\overline{\Omega},k\in\overline{\Omega}\right\}$.

c. The set of performance indices $P^{(j)}$ is assembled consisting of $P\left[j;m,;k,k\right]$ evaluated for all $b_{j,}^{(m)}\in B^{(j)}$ and $t_{j,k,k}\in T^{(j)}$.

d. The first tow-path segment $t_{j,k,k}\in T^{(j)}$ selected is that for which $P\left[j;m,;k,k\right]$ for some $\left\{m,\right\}$ has the largest magnitude among all the elements of $P^{(j)}$. In subsequent iteration, which is continued until all n_{weft} tow paths have been determined, the next segment selected is that for which $P\left[j;m,;k,k\right]$ for some $\left\{m,\right\}$ is the next largest in $P^{(j)}$, subject to the restrictions that:

- no candidate tow-path segment $t_{j,k,k}$ can be selected for which either k or k already appears in a selected tow-path segment; and
- no candidate tow-path segment can be selected if the background vector $b_{j,}^{(m)}$ referenced in evaluating $P\left[j;m,;k,k\right]$ has already been referenced in evaluating $P\left[j;m,;k,k\right]$ for some already-selected tow-path segment.

Since the length of $\overline{\Omega}$ is n_{weft}, there are n_{weft}^2 candidate tow-path segments to be assessed between intersections o_j and o_{j+1} in the procedure described above. As for the total number of background vectors to be matched against each candidate tow-path vector: there are five instances of $m\in\left\{L,t,z,b,s\right\}$ for which $\in\overline{\Omega}$ and two for which $\in\acute{\Omega}$, and the length of $\acute{\Omega}$ is $n_{weft}+1$; and thus there are $5n_{weft}+2\left(n_{weft}+1\right)$ background vectors. Hence, the length of $P^{(j)}$ is $n_{weft}^2\left(5n_{weft}+2\left(n_{weft}+1\right)\right)=2499$ for the exemplar with $n_{weft}=7$. Searching $P^{(j)}$ for the seven elements of largest magnitude is a modest computational task.

Selected tow-path segments are added to the tow-path records τ_w. When design of a 2D section is complete, the set of tow path records $T_{weft}^{(i)}=\left\{\tau_w\middle|w=1,\ldots,n_{weft}\right\}$ for the i^{th} 2D weft section or $T_{warp}^{(j)}=\left\{\tau_w\middle|w=1,\ldots,n_{warp}\right\}$ for the j^{th} 2D warp section is added to the 3D architecture set

$$T_{3D}=\left\{T_{weft}^{(i)}\middle|i=1,\ldots,N_{weft}\right\}\cup\left\{T_{warp}^{(j)}\middle|j=1,\ldots,N_{warp}\right\} \tag{10}$$

which constitutes the entire topological definition of the 3D weave design.

Alongside the record τ_w of Eq. (8c), a record of the values of the performance index associated with each selected tow segment has potential value:

$$P_{3D}=\left\{P_{weft}^{(i)}\middle|i=1,\ldots,N_{weft}\right\}\cup\left\{P_{warp}^{(j)}\middle|j=1,\ldots,N_{warp}\right\} \tag{11a}$$

$$P_{weft}^{(i)}=\left\{p_w\middle|w=1,\ldots,n_{weft}\right\} \quad \text{(for the } i^{\text{th}} \text{ 2D weft section)} \tag{11b}$$

$$P_{warp}^{(i)}=\left\{p_w\middle|w=1,\ldots,n_{warp}\right\} \quad \text{(for the } j^{\text{th}} \text{ 2D warp section)} \tag{11c}$$

where p_w for the paradigm for a 2D weft section is defined by $p_w=\left\{P\left[j;m,;\tau_j^{(w)},\tau_{j+1}^{(w)}\right]\middle|j=1,\ldots,N_{warp}-1\right\}$, with $\left\{\tau_j^{(w)},\tau_{j+1}^{(w)}\right\}$ the selected $\{k,k\}$ and $\{m,\}$ the indices for the background vector involved in the selection.

5. Sampling the scope of the BVM design space

The paradigm of the BVM exhibited in Sec. 3 has reduced the design space for the architecture of a 3D weave to the five scalar weights $\left\{c_m,m\in\{L,t,z,b,s\}\right\}$. Yet the aptness of the background fields and the diversity of the architectural targets they represent allows the BVM, even in this minimal form, to generate periodic and non-periodic designs that respond plausibly to various loading scenarios.

In the examples of this section, the parameters $\{c_m\}$ are selected by hand to tune designs and a threshold parameter is introduced that allows the creation of cavities or voids. The examples consider the design of one or several 2D weft sections.

5.1 Periodic patterns from generic background vectors

The generic background vectors defined in Sect. 4, being invariant along the 2D weft section (i.e., along the y-direction), tend to generate periodic designs when they act alone. In the following illustrations, the weights $\{c_t,c_z,c_b,c_s\}$ are available for tuning, while $c_L=0$.

Prioritizing in-plane and through-thickness reinforcement can lead to a non-woven orthogonal laminate or an orthogonal interlock weave, while prioritizing shear reinforcement can generate a through-thickness angle interlock weave (Fig. 5(a-c)). A hybrid design that combines orthogonal interlock and layer-to-layer angle interlock reinforcement in the through-thickness direction is found by tuning a combination of through-thickness and bending reinforcement priorities (Fig. 5(d)). Note that in this last case, the centre region has fewer straight tows than the orthogonal interlock weave of Fig. 5(b), the centre region in bending having low in-plane loading.

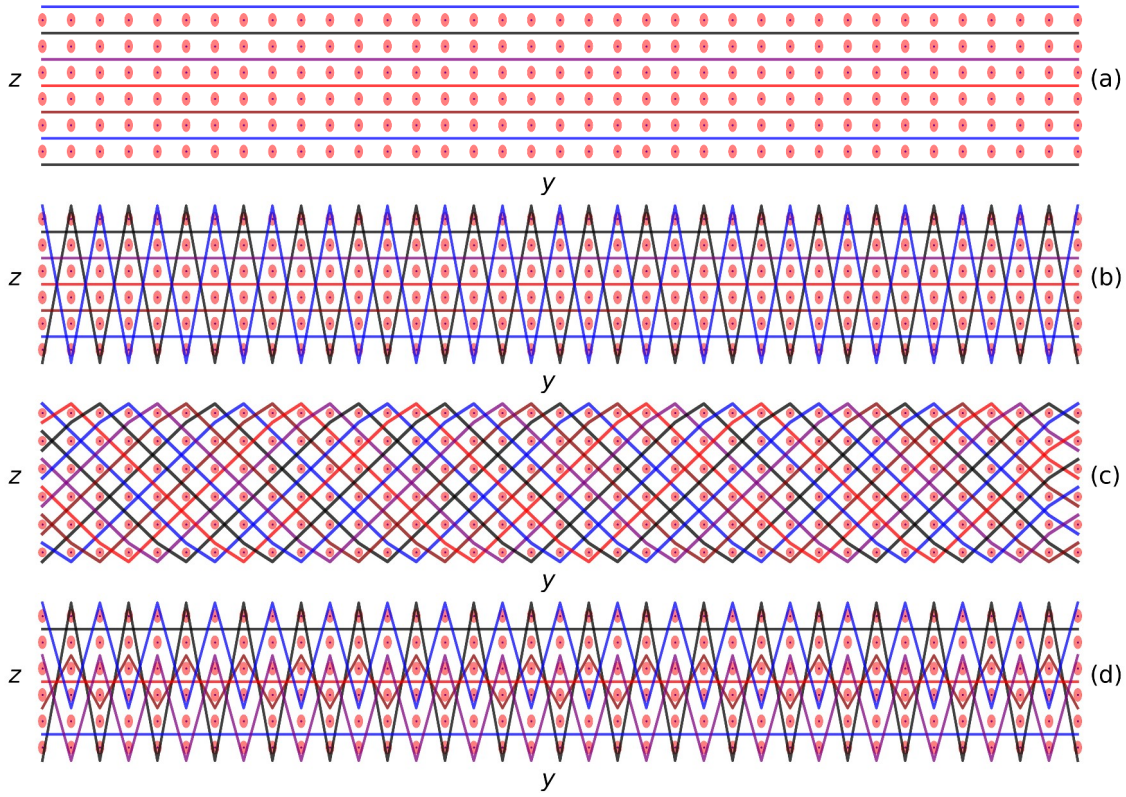

Figure 5. Familiar designs re-created by the listed combinations of weights, with $c_L = 0$ in all cases. (a) orthogonal non-woven laminate ($c_t = 1.0$, $c_z \leq 1.0$, $c_b = 0.1$ $c_s = 0.1$); (b) orthogonal interlock weave ($c_t = 0.9$, $c_z = 1.0$, $c_b = 0.1$, $c_s = 0.1$); (c) through-thickness angle interlock weave ($c_t = 0.1$, $c_z = 0.1$, $c_b = 0.1$, $c_s = 1.0$); (d) hybrid orthogonal interlock and layer-to-layer angle interlock ($c_t = 0.1$, $c_z = 1.0$, $c_b = 0.9$, $c_s = 0.1$). In (c), the history parameters α and β of Eq. (9b) also take small non-zero values, $\alpha = \beta = 0.001$. Ordering restriction $\overline{O} = \overline{O}^{(alt)}$ in cases (a), (b), and (d) and $\overline{O} = \overline{O}^{(1,2)}$ in case (c).

5.2 Bespoke background vectors lead to non-periodic patterns

Bespoke background vectors, commonly being spatially heterogeneous, generate non-periodic designs that tend to match patterns of load paths in the structure, but with useful variability when balanced against different generic background vectors. In the following illustrations, the weights $\{c_L, c_t, c_z, c_b, c_s\}$ are all available for tuning.

Three common plane problems in topology optimization research are studied here: a cantilevered beam subject to a point load at the unclamped end; a beam subject to a central point load with simple end supports; and a beam subject to a central point load with one simple end support and one free roller support

located at $\frac{4}{5}$ of its length (Fig. 6). Principal stress components were determined by executing a 2D isogeometric analysis with a mesh of 50×10 covering an elastically isotropic beam of dimensions 120 × 20 mm, with Young's modulus 70 GPa, Poisson's ratio 0.3, and a point load of magnitude 500 N. Contour plots of the von Mises stress appear in Fig. 6. Principal stresses evaluated at the grid of reference points $r_{j,k}^{(b)}$ (Fig. 6) are converted to bespoke background vectors, which, by the normalization of Eq. (4), are dimensionless quantities of magnitude bounded by unity.

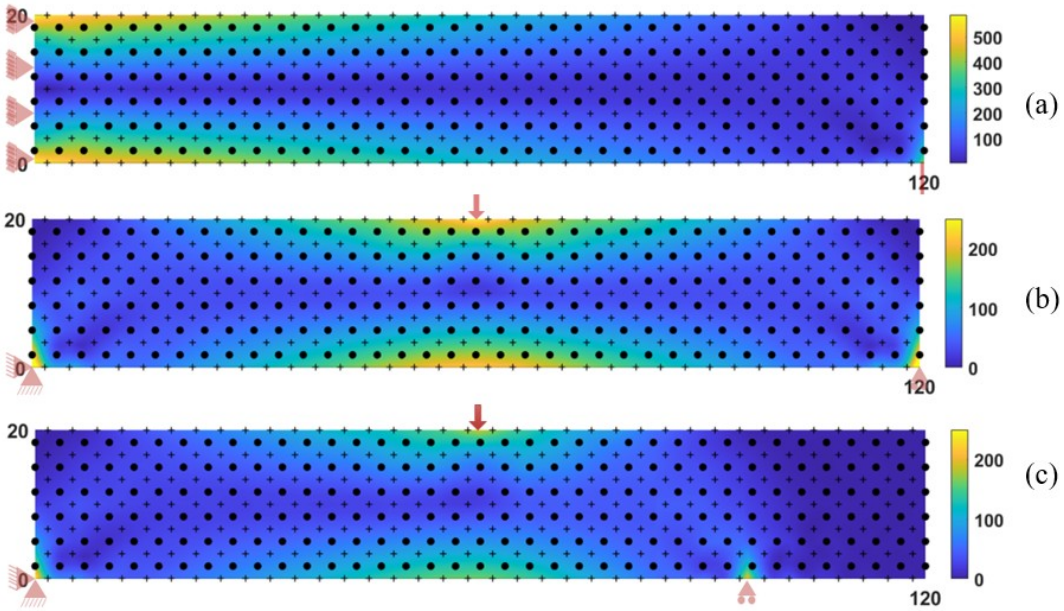

Figure 6. The Von Mises stress distributions in (a) a cantilevered beam; (b) a beam in symmetric three-point bending; and (c) a beam in asymmetric three-point bending. Load and supports as indicated. Black circles indicate the positions of warp tows for textile design, aligned vertically at each intersection o_j. Crosses indicate the positions of the reference points $r_{j,k}^{(b)}$ at which bespoke background vectors are defined.

A sequence of designs controlled by bespoke background vectors was generated for 2D weft sections containing seven or 12 weft tows (available weft tow locations $\overline{\Omega}$ given by Eq. (3b)) by assigning $c_L = 1$ with all of $\{c_t, c_z, c_b, c_s\}$ taking near-zero values (10^{-3} to order of magnitude). The resulting designs are characterized by tows following load paths (the bespoke background vector of greater magnitude at every reference point) and resemble known topology optimization solutions for these standard problems (Figs. 7 and 8).

With more weft tows available in the 2D section for design, the diversity of the allocation of tows to in-plane and through-thickness orientations increases as later-assigned tows match bespoke vectors of lesser magnitude (Fig. 8 vs. Fig. 7). Even though the generative algorithm acts sequentially in one direction, for the cases with $\overline{O}_{i,j}^{\langle alt \rangle}$, the directional bias of the designs for the symmetric three-point bending case may not be obvious, with symmetric design output illustrated in Fig. 7(b). However, for the cases with $\overline{O}_{i,j}^{\langle 1,2 \rangle}$, the symmetry of the design output cannot be guaranteed. This is because at the same weft tow location, there are two candidate tows. At each local stack interval, the two candidates have equal chance (may have the same P value) to select the same location in the next warp stack location. This also means that performing the algorithm inversely in the same interval, the designs could be different. The extra history term added in Eq. (9a) may change the P values slightly, but the next step design is still highly dependent on the previous steps. This can be seen from the results shown in Fig. 8(b) with an asymmetric design output.

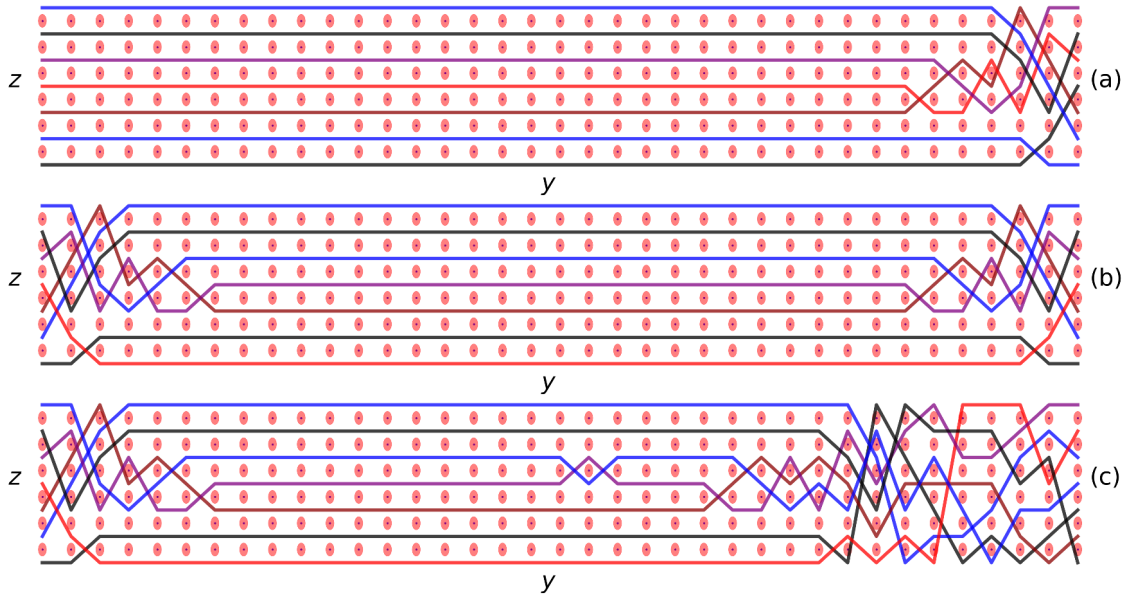

Figure 7. Weave designs for seven weft tows dominated by bespoke background vectors ($c_L = 1$; $c_z = 0$; $c_t = c_b$ ¿ $c_s = 0.001$): (a) cantilevered beam. (b): symmetric three-point bending; (c) asymmetric three-point bending. Ordering restriction $\overline{O} = \overline{O}^{\langle alt \rangle}$ in all cases.

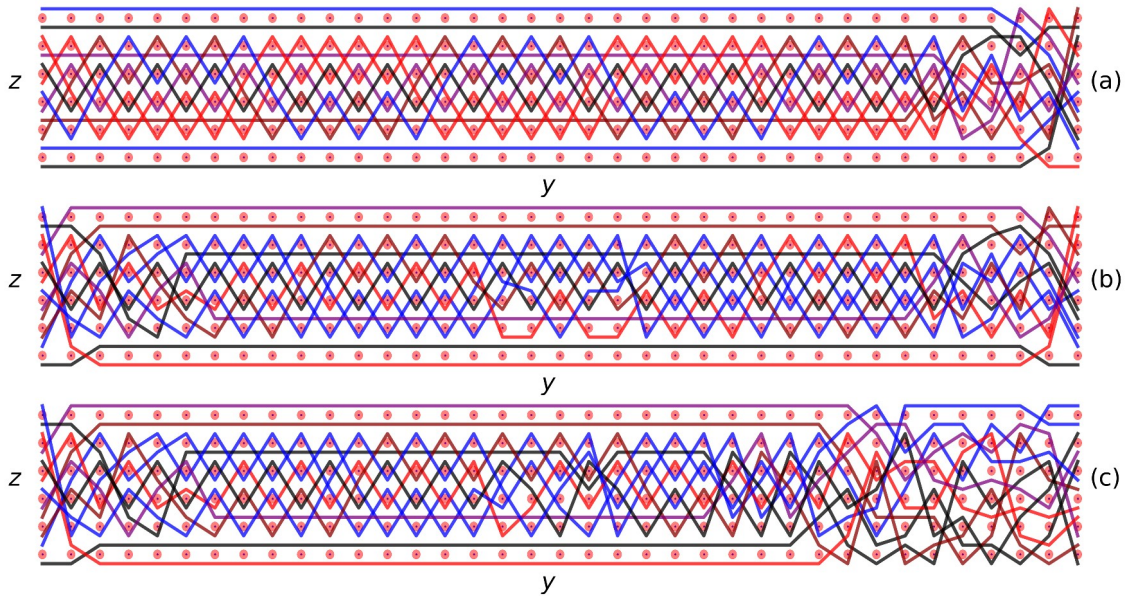

Figure 8. Weave designs for seven weft tows dominated by bespoke background vectors ($c_L=1$; $c_z=0$; $c_t=c_b¿c_s=0.001$). (a): cantilevered beam. (b): symmetric three-point bending. (c): asymmetric three-point bending. Ordering restriction $\overline{O}=\overline{O}^{(1,2)}$ in all cases.

5.3 Multiple design objectives: tuning bespoke and generic background vectors

The bespoke background vectors, being based on elastic stress field calculations, carry no information about potential failure mechanisms for the component. One common failure mechanism is delamination. The BVM can generate designs that have the potential of balancing the matching of elastic stress fields (for global stiffness) and protecting against delamination by tuning bespoke and generic background vectors. In the next sequence of designs, bespoke background vectors and through-thickness generic background vectors are tuned by manipulating $\{c_L, c_z\}$ while $\{c_t, c_b, c_s\}$ remain very small.

Figs. 9 – 12 show how the relative content of through-thickness tows increases as the weight c_z increases while $c_L=1$ (and compare with the case $c_z=0$ in Figs. 7 and 8). With increasing c_z, the through-thickness content rises first where the bespoke background vectors have smaller magnitude (regions of low von Mises stress in Fig. 6), then extends progressively over the entire component.

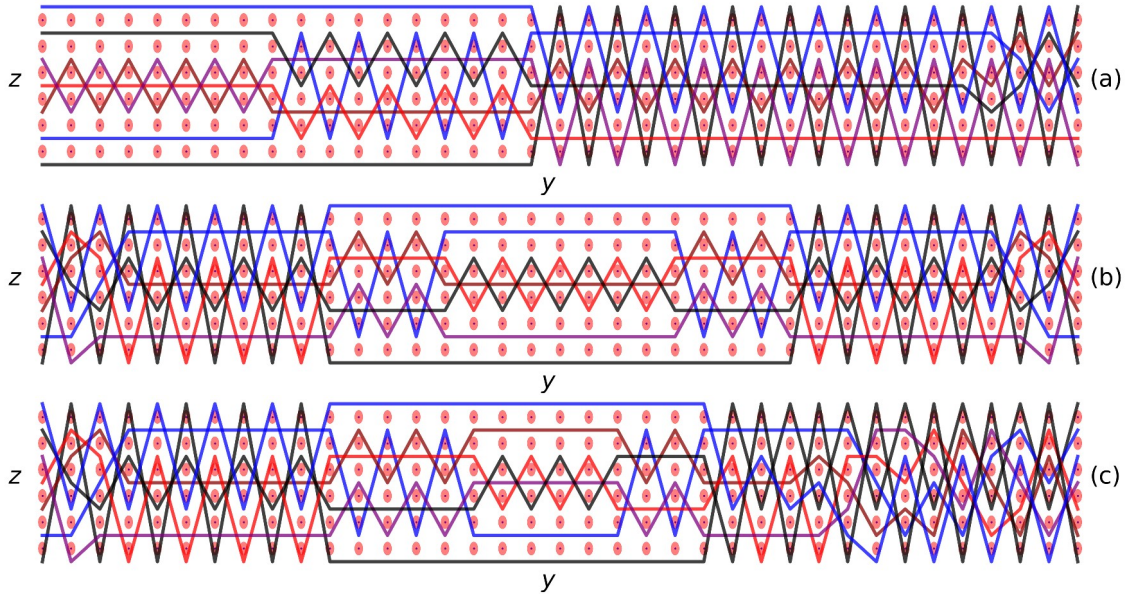

Figure 9. Weave designs for twelve weft tows influenced by bespoke background vectors only ($c_L=1$; $c_z=0.5$; $c_t=c_b¿c_s=0.001$). (a): cantilevered beam. (b): symmetric three-point bending. (c): asymmetric three-point bending. Ordering restriction $\overline{O}=\overline{O}^{(alt)}$ in all cases.

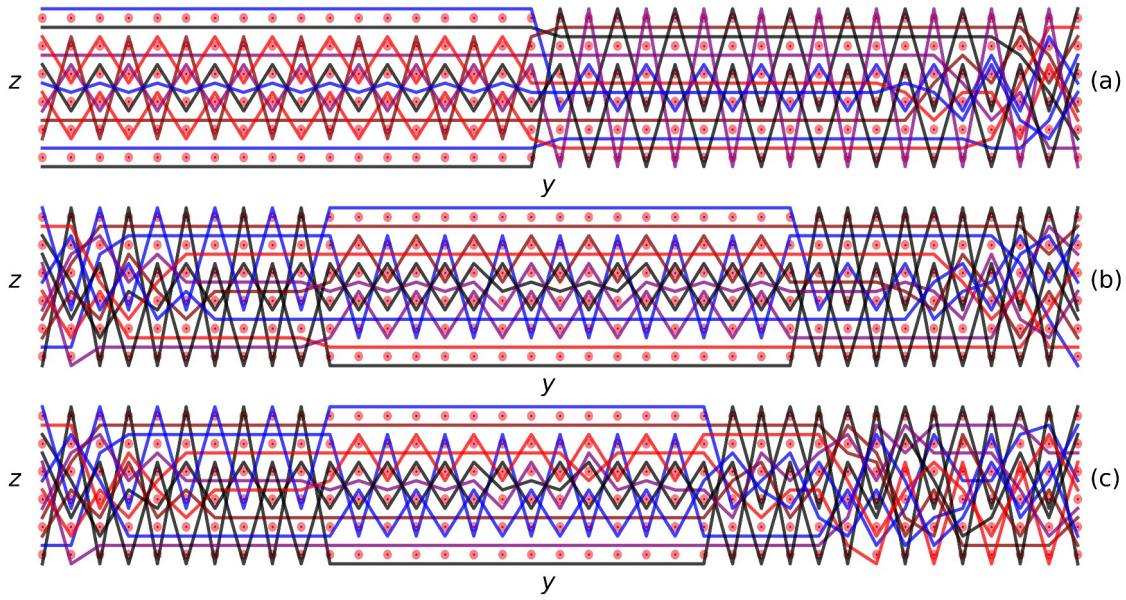

Figure 10. Same as Fig. 9 ($c_L=1$; $c_z=0.5$; $c_t=c_b¿c_s=0.001$), but with 12 weft tows. Ordering restriction $\overline{O}=\overline{O}^{(1,2)}$ in all cases.

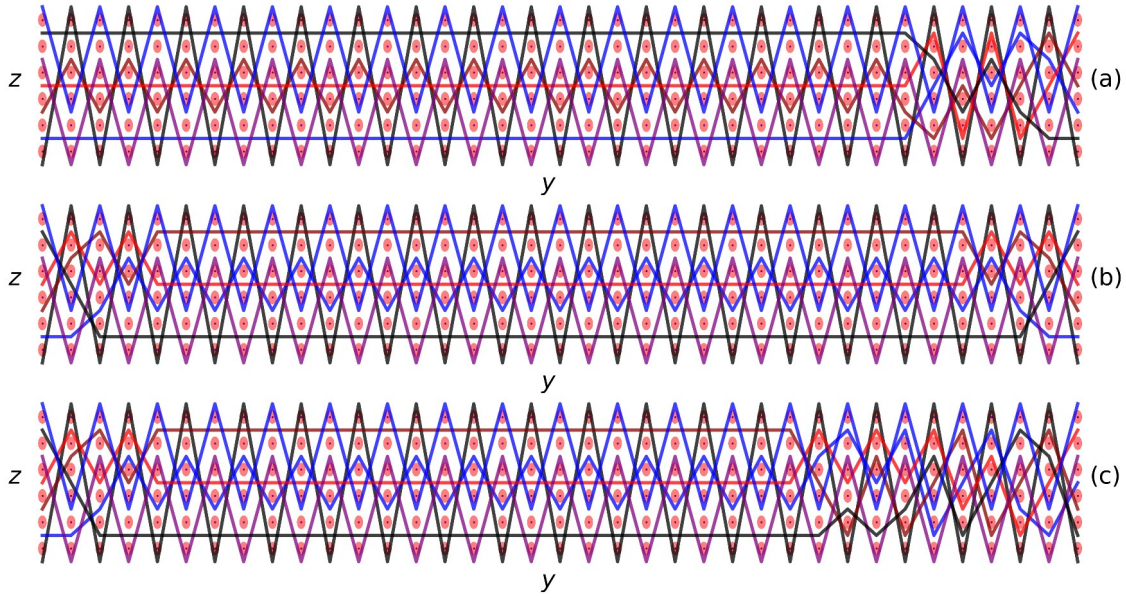

Figure 11. Weave designs for seven weft tows influenced by bespoke and generic through-thickness background vectors ($c_L=1\,;\,c_z=1.5;\,c_t=c_b¿c_s=0.001$). (a): cantilevered beam. (b): symmetric three-point bending. (c): asymmetric three-point bending. Ordering restriction $\overline{O}=\overline{O}^{(alt)}$ in all cases.

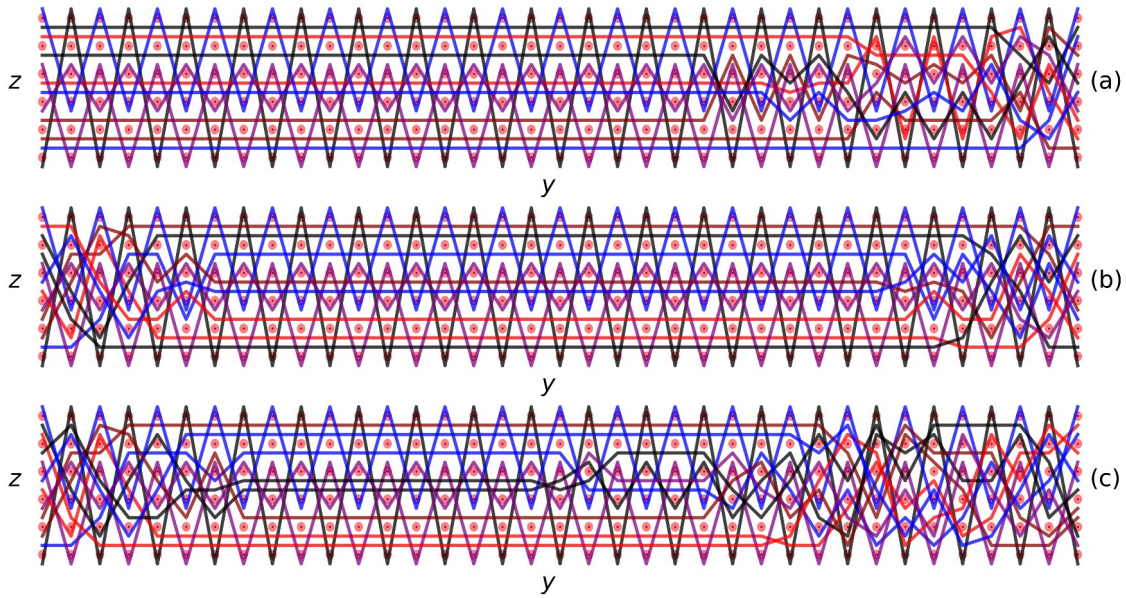

Figure 12. Same as Fig. 11 ($c_L=1\,;\,c_z=1.5;\,c_t=c_b¿c_s=0.001$), but with but with 12 weft tows. Ordering restriction $\overline{O}=\overline{O}^{(1,2)}$ in all cases.

5.4 Tow deletion: the formation of void spaces

The reinforcing performance index P of Eq. (9) carries information that can potentially be exploited in generating designs with advanced functionality. Consider further the design of Fig. 12(b), which

balanced the influence of expected load paths and enhanced delamination resistance. In the generated designs, some tows contribute relatively strongly to at least one of the nominal design preferences, others less so. Following completion of the design, the weaker contributors can be identified by the criterion $mean\left[p_w\right] < P_{del}$ where p_w is the record of P values of Eq. (11) and $P_{del} < 1$ is a threshold parameter, which, in applications, can be made available to an optimizing algorithm.

By selecting the value of P_{del}, first the two weakest contributing weft tows in Fig. 12(b) were identified and deleted from the final design, all other tows remaining as they were; and then, by increasing P_{del}, the next two weakest contributors were also deleted (Fig. 13). The resulting designs are tending towards a rudimentary sandwich structure, which might perform well in bending while still having through-thickness integrity. The deletions lower the total mass, favouring mass-normalized performance. The deletion step mimics the use of sacrificial tows in processing, which are woven into the weave and then removed from the final product, e.g., by chemical etching or heat, often after the fibre preform has been consolidated with a matrix, which fixes the geometry of all other tows (e.g., [19]).

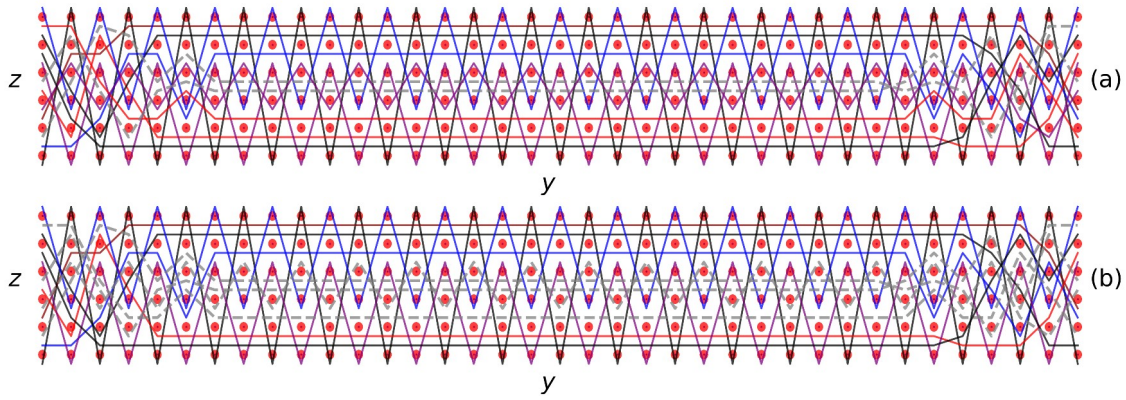

Figure 13. Tow deletion applied to Fig. 12 (b) with (a) two and (b) four tows deleted. The deleted tows are plotted with dashline style.

5.5 Different 2D sections in a 3D structure

As an elementary illustration of the design of multiple 2D sections within a 3D structure, consider a 3D cantilevered beam with a point load applied at one corner of the free end (Fig. 14). Three weft sections (y-z planes) are analyzed, namely the two side surfaces and the mid-plane. Since the loading is asymmetric, the stresses on the three sections differ. Principal stress fields are extracted for each section from a 3D FEM

analysis, using the same model characteristics used for the plane beam problems described above extended to a third dimension of length 20 mm. The FEM analysis is performed using isogeometric analysis with Non-Uniform Rational B-Splines (NURBS) bases as shape functions. There are $8 \times 8 \times 40$ brick elements with quadratic shape functions. Bespoke background vectors are built from the principal stresses according to Eq. (4), but now with distinct fields resulting for each 2D section.

Designs dominated by the bespoke background vectors ($c_L = 1$; $\{c_t, c_z, c_b, c_s\}$ very small) differ for the three sections in a manner reflective of the different proportions of bending and shear loads expected in the 3D structure (Fig. 15). When the bespoke and generic through-thickness background vectors are both given influence ($c_L = 1; c_z = 4.56$; $\{c_t, c_b, c_s\}$ remaining very small), the three sections continue to differ from one another, but all three now contain increased proportions of through-thickness reinforcement (Fig. 16).

With the section-by-section design approach, it is possible to generate 3D woven structures tailored for heterogeneous loading conditions. The examples of this section have displayed an encouraging variety of designs, obtained by manipulating only the five degrees of freedom offered by the set of weights $\{c_m | m \in \{L, t, z, b, s\}\}$ plus a single deletion threshold. The basis functions represented by the combination of bespoke and generic background vector fields form an efficient design space.

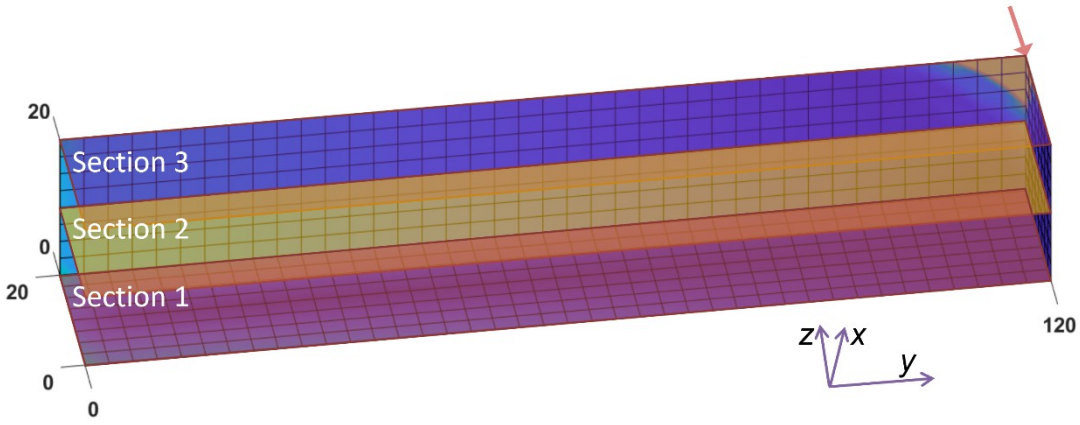

Figure 14. A 3D cantilever beam with built-in left end and a point load applied at one corner of the free end. Designs are generated for the marked 2D sections 1, 2, and 3, with the point load acting on Section 3.

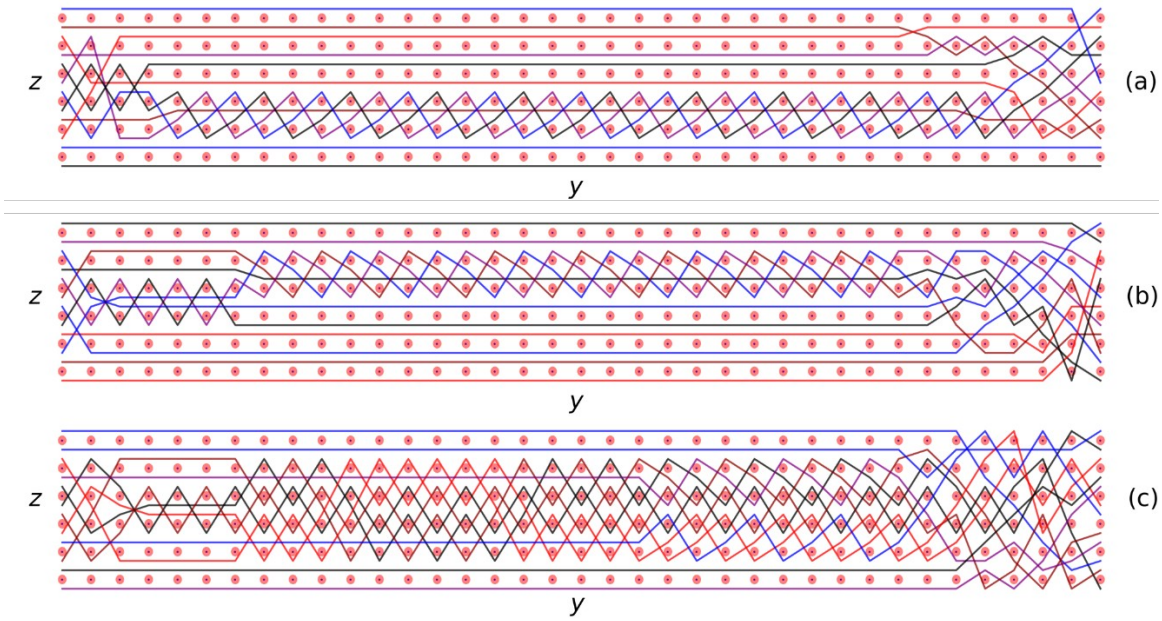

Figure 15. Weave designs for the sections of Fig. 14 using 12 weft tows influenced by bespoke background vectors only ($c_L=1$; $\{c_t, c_z, c_b, c_s\}$ very small): (a) for Section 1, (b) for Section 2, and (c) for Section 3 (loaded section). Ordering restriction $\overline{O}=\overline{O}^{(1,2)}$ in all cases.

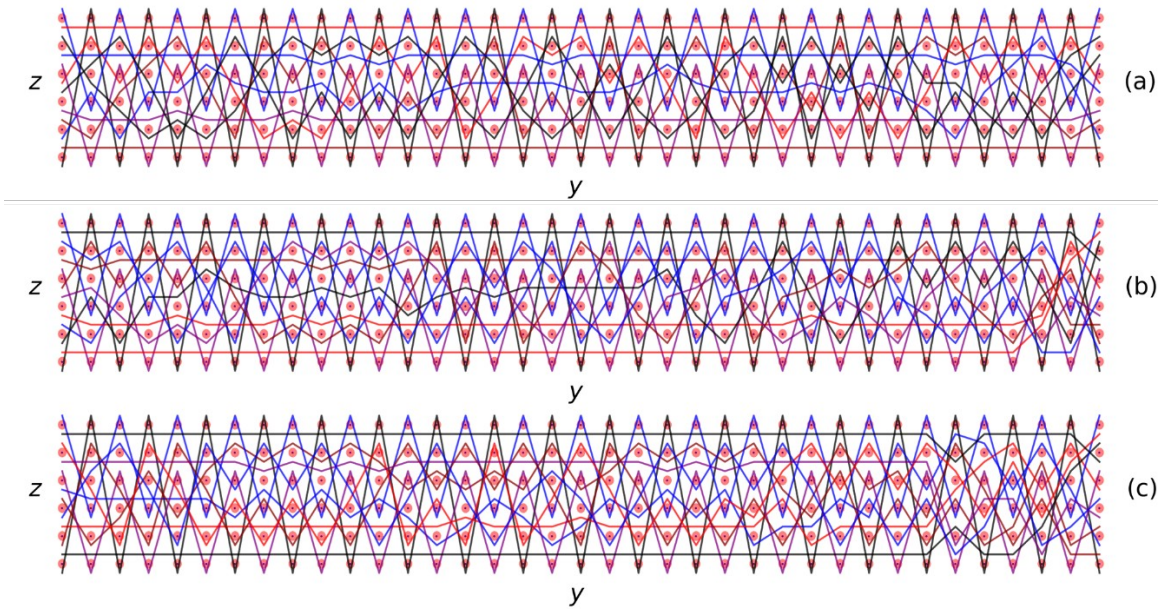

Figure 16. Same as Fig. 15 but with weft tow designs influenced by a balance of bespoke and generic through-thickness background vectors ($c_L=1; c_z=4.56$; $\{c_t, c_b, c_s\}$ very small).

6 Generalizations

6.1 Possible use of the BVM within an optimization engine

Consider the BVM embedded in some optimization engine (Fig. 17). The BVM design space as defined above offers three types of parameters to the optimizer:

I. The weights $\{c_m | m \in \{L, t, z, b, s\}\}$ associated with the total background vector set, with $c_m \geq 0$.

II. The threshold for tow deletion P_{del} of Eq. (9a).

III. The ordering restrictions $\{\overline{O}_{i,j} | i = 1, \ldots, N_{weft}; j = 1, \ldots, N_{warpweft}\}$.

Objective functions, such as the total mass of the component, its stiffness, and its critical loads, will be evaluated by analysis of a 3D model built from T_{3D} of Eq. (10) for the current optimization iteration. The 3D model will be heterogeneous, the reinforcement architecture being represented explicitly. Since bespoke background vectors were defined initially using a homogeneous-material model, re-computation using the more accurate heterogeneous-material model may be beneficial during optimization iteration.

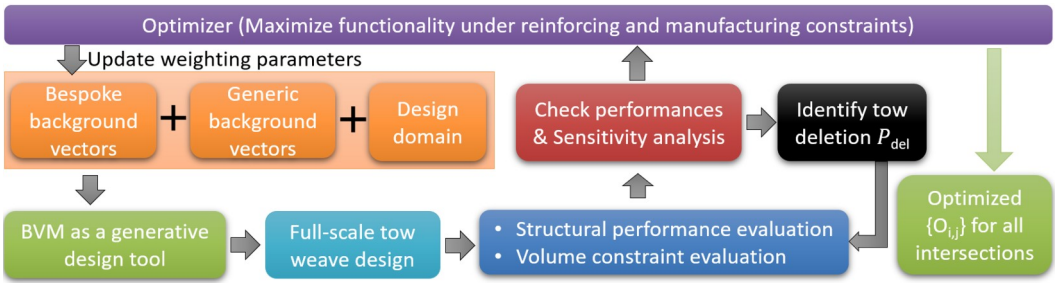

Figure 17. The BVM within an optimization scheme.

6.2 Expanding the design space

The designs found in Sect. 5 using just the five degrees of freedom available among the weights $\{c_m | m \in \{L, t, z, b, s\}\}$ plus the single threshold P_{del} are encouragingly varied, but general applications will require design spaces with many more degrees of freedom. The structure of the BVM *said below* allows systematic design space expansion, effectively without limit, while always exploiting the aptness of the BVM paradigm.

6.2.1 The weights c_m

The weights $\{c_m | m \in \{L, t, z, b, s\}\}$ can be generalized by allowing each c_m to be a function of 2D-

section type and spatial position: $c_m = c_m[q, i, j]$ where $q \in \{warp, weft\}$ and $\{i, j\}$ tags an intersection $o_{i,j}$. For example:

- Dependence on q opens the possibility of warp and weft tows being assigned different primary responsibilities, e.g., warp remaining primarily straight to maximize in-plane properties while weft traverse through-thickness to inhibit delamination.
- Dependence on $\{i, j\}$ opens the possibility of generating weave types not exemplified in Sect. 5. For example, an architecture featuring long intervals of straight in-plane weft tows punctuated by brief intervals where the weft tows move through the thickness (e.g., a satin weave) can be generated by building that spatial pattern into the parameters c_t and c_z, the weights for the "in-plane" and "through-thickness" generic background vectors, Eqs. (5a) and (5b).

One might also allow each c_m to be a function of the index k in the background reference point $r_{j,k}^{(b)}$, but dependence on k (or z) is already available via the definition of the background vectors; separate dependence of c_m on k is likely to be superfluous.

Implementing dependence of $\{c_m[q] | q \in \{warp, weft\}\}$ on $\{i, j\}$ amounts to a search during optimization for advantageous spatial patterns in the individual c_m. The BVM has transformed the relatively cumbersome problem of probing a design space defined in terms of all possible orderings $\{O^{(i,j)} | i = 1, \ldots, N_{weft}; j = 1, \ldots, N_{warp}$ ¿¿ that comply with the restrictions $O^{(i,j)} \in \overline{O}$, which is still practically unbounded even given the restrictions, into a relatively convenient search for patterns in the $\{c_m\}$ defined on a discrete rectangular grid (the pixel array $\{i, j\}$ of dimensions $N_{warp} \times N_{weft}$).

Experience in 3D weave design suggests that both non-periodic and periodic patterns will be useful. Note, however, that periodic patterns in $\{c_m[q] | q \in \{warp, weft\}\}$ do not imply that the resulting architecture is necessarily periodic, because the background vector field is not periodic. A blend of periodic and non-periodic candidates defined on $\{i, j\}$ may be amenable to compact representation by discrete Fourier transforms. While dependence of $c_m[q, i, j]$ on $\{i, j\}$ may be chosen differently for different tow type q, the patterns $c_m[weft, i, j]$ and $c_m[warp, i, j]$ must generally be correlated.

6.2.2 Thresholds

The threshold condition Eq. (12) is readily amenable to generalization. The parameter P_{del} can be made spatially heterogeneous (applied only to subsets of tows); and other threshold conditions might be introduced, e.g., one that seeks conditions where it may be advantageous to augment the size of a tow that is well aligned with tow paths, with an associated parameter P_{aug}.

6.2.3 Varying tow numbers within stacks

Given any array of ordering restrictions $\left\{ \overline{O}^{(i,j)} \middle| i=1,\ldots,N_{weft}\,;\, j=1,\ldots,N_{warp} \right\}$ for n_{weft} and n_{warp} tows per intersection, the paradigm of the BVM exhibited in Sect. 4 can be generalized to permit the number of weft or warp tows in any 2D weft or warp section to be any number n_{weft} or n_{warp} satisfying $1 \le n_{weft} \le n_{weft}$ or $1 \le n_{warp} \le n_{warp}$, respectively, with n_{weft} and n_{warp} now denoting upper bounds imposed by a given choice $\overline{O}^{(i,j)}$ (Fig. 2). Which is to say, available weft or warp positions in the ordering $\overline{O}^{(i,j)}$ can be left unoccupied. The BVM would be executed with trivial modification; and a consolidation step in the building of the 3D model used for objective evaluation would close gaps.6.2.4 De-restricting orderings

Many existing 3D weave designs are consistent with the restriction of the ordering of warp and weft tows at intersections designated by $\overline{O}^{(alt)}$ and $\overline{O}^{(1,2)}$, provided the number of tows per stack is generalized as in the preceding paragraph. However, the design of multi-functional structures with non-uniform geometry might benefit from more varied orderings. For example, sacrificial tows of one type (warp or weft) can form internal cavities whose dimensions are multiple tow thicknesses when they are allowed to be ordered in multi-tow blocks within intersections [18].

Most generally, the ordering restriction $\overline{O}^{(i,j)}$ applied to any intersection $o_{i,j}$ can vary with any desired spatial dependence on $\{i,j\}$. Any change in an $\overline{O}^{(i,j)}$ is effected by changing the integers listed in $\overline{\Omega}$ of Eq. (3b). However, varying n_{warp} or n_{weft} in any stack and deleting select tows already gives much variability in ordering, suggesting that variations in ordering restrictions might be unnecessary or at most should be introduced sparingly.

6.3 The viability of designs

When a complex 3D design is optimized, it may yet prove not to be viable, e.g., because tows are too tortuous or are too unevenly packed for the design to be realized as a robust fabric on a loom. Constraints

will generally be required to assure a design conforms with manufacturing reality. The generalizations of the BVM listed above will be required to support application of the required constraints.

Consider, for example, the non-uniform spatial density of tows in the designs of Figs. 7 – 9, a possible cause of difficulty in the beat-up operation during fabrication (Fig. 1) and post-fabrication handing. Generalizing the number of weft tows in a weft stack allows the multi-tow designs of a single weft section (Figs. 7 – 9) to be devolved among multiple successive weft sections, relieving possible entanglement and excessive deformation of tows during beat-up. Spatial variations in $c_m[q,i,j]$ permit the density of weft tows averaged over multiple successive weft sections to be constrained to be close to spatially uniform (independent of coordinates y and z). Uniform density on $\{y,z\}$ when averaged over an appropriate gauge length along x will promote dense packing during beat-up and ease of handling of the fabric when removed from the loom.

6.4 Locking the fate of tows during optimization

On every iteration of optimization, the BVM generates a new record of the reinforcement performance indices P_{3D} of Eq. (11) covering every tow in the 3D design. The deletion criterion of Eq. (12) exemplified the possible use of the information in P_{3D} to minimize mass.

The most accurate decisions on tow deletion would use the stress field computed for the final optimized design. However, it may prove that heuristic algorithms based on P_{3D} sampled during iteration towards optimization can be trained to predict in early iterations whether a tow will ultimately be deleted.

It may similarly prove that P_{3D} is an early predictor of whether the locus of one tow will remain in its current form in the final optimized design; or whether a tow will be selected for augmentation in the final optimized design. Any early prediction of any tow's fate allows that tow to be fixed, reducing the degrees of freedom still in play. Thus, the detailed information in P_{3D} may support a physics-informed heuristic algorithm within the overarching optimization that expedites optimization while maintaining sufficient accuracy.

6.5 Invariance of the BVM under design space expansion

Whatever spatial pattern is trialed for the $\{c_m\}$, whatever threshold conditions are specified, whatever tow numbers are used in stacks, and whatever set of ordering restrictions $\{\overline{O}_{i,j}\}$ is chosen, the definition of

the BVM remains unaltered. Provided the ordering restrictions $\left\{\overline{O}_{i,j}\right\}$ remain fixed within a design iteration, designs for 2D sections can be generated independently of one another. Any spatial variations in $\left\{c_m\right\}$ are trivially incorporated in Eq. (9b). And all designs the BVM generates in an expanded design space will remain legal in the sense defined by the rules of operation of the 3D weaving loom [18].

7. Concluding remarks

The background vector method (BVM) offers a compact yet flexible representation of the design space available to integral 3D woven architectures for large-scale structures. By devolving a 3D preform design into an ensemble of independent 2D section designs, each of which can be realized by a simple algorithm executed sequentially along a section like a multi-agent game, the BVM achieves very high computational efficiency: seconds of computational time sufficed for any of the example cases in Sect. 5, using a non-optimized code on a contemporary laptop computer. The speed of the BVM will support large-scale design optimization.

By defining spatial patterns in the weights $\left\{c_m[q]\middle| q \in \{warp, weft\}\right\}$ and in the restricted orderings $\left\{\overline{O}_{i,j}\right\}$ of increasingly fine granularity on the discrete spatial grid $\{i, j\}$, one can in principle regain access to the entire design space defined by the unrestricted orderings $\left\{O_{i,j}\right\}$, whose (infeasible) size is given by Eq. (2b).

The structure of the BVM is readily integrated into a standard gradient-based or heuristic optimization algorithm, using the weights and thresholds as design variables. The values returned for the performance indices associated with selected tow segments P_{3D} during an iteration towards optimization are intuitively attractive parameters for exploitation within a physics-informed machine-learning optimization approach.

Replication of results & Conflict of interest

All data are provided in the manuscript. Extra information can be made available upon request. The authors have no competing interests to declare that are relevant to the content of this article.

Acknowledgments

This research is supported by A*STAR <C210112026>.

References

[1]. Behera, B. and Dash, B., (2015) Mechanical behavior of 3D woven composites, Mat. & Des., 67: 261–

271.

[2]. Chen, X., Taylor, L. W., and Tsai, L.-J., (2011) An overview on fabrication of three-dimensional woven textile preforms for composites, Text. Res. J., 81: 932–944.17

[3]. Bilisik, K., (2012) Multiaxis three-dimensional weaving for composites: a review, Text. Res. J., 82: 725–743.

[4]. Gereke, T., Dobrich, O., Hubner, M., and Cherif C., (2013) Experimental and computational composite textile reinforcement forming: A review, Compos. Part A Appl., 46: 1–10.

[5]. Carvelli, V., and Lomov, S. V., (2015) Fatigue damage evolution in 3D textile composites, in: Fatigue of textile composites, Elsevier, pp: 223–253.

[6]. Chen, X., Chen, L., Zhang, C., Song, L., and Zhang, D., (2016) Three-dimensional needle-punching for composites–a review, Compos. Part A Appl. 85: 12–30.

[7]. Elmogahzy, Y. E., (2019) Engineering textiles: Integrating the design and manufacture of textile products, Woodhead Publishing.

[8]. Mehdikhani, M., Gorbatikh, L., Verpoest, I., and Lomov, S. V., (2019) Voids in fiber-reinforced polymer composites: A review on their formation, characteristics, and effects on mechanical performance, J. Compos. Mater., 53: 1579–1669.

[9]. Bodaghi, M., Lomov, S., Simacek, P., Correia, N., and Advani, S., (2019) On the variability of permeability induced by reinforcement distortions and dual scale flow in liquid composite moulding: A review, Compos. Part A Appl., 120: 188–210.

[10]. Mouritz, A. P., Bannister, M. K., Falzon, P., and Leong, K., (1999) Review of applications for advanced three-dimensional fibre textile composites, Compos. Part A Appl., 30: 1445–1461.

[11]. Karaduman, N. S., Karaduman, Y., Ozdemir, H., and Ozdemir, G., (2017) Textile reinforced structural composites for advanced applications, Textiles for advanced applications 87.

[12]. Huang, T., Wang, Y., and Wang, G., (2018) Review of the mechanical properties of a 3D woven composite and its applications, Polym Plast Technol Eng, 57: 740–756.

[13]. Saboktakin, A., (2019) 3D textile preforms and composites for aircraft strcutures: A review, Int. J. Aviat. Aeronaut. Aerosp., 6:2.

[14]. Desplentere, F., Lomov, S. V., Woerdeman, D., Verpoest, I., Wevers, M., and Bogdanovich, A., (2005)

Micro-CT characterization of variability in 3D textile architecture, Compos Sci Technol, 65: 1920–1930.

[15]. Long, A. C., (2005) Design and manufacture of textile composites, Elsevier.

[16]. Chen, X., (2009) Modelling and predicting textile behaviour, Elsevier.

[17]. Cox, B., Yang, Q., Marshall, D., and Davis, J., (2005) Design issues in using integral textile ceramic composites in turbine engine combustors, J. Propuls. Power., 21: 314–326.

[18]. Cox, B. N., Nilakantan, G., Sudre, O., and Marshall, D. B., (2016) Generating virtual specimens for complex non-periodic woven structures by converting machine instructions into topological ordering rules, Compos. Struct. 141: 63–78.

[19]. Marshall D. B. and Cox B. N., (2008) Integral textile ceramic structures, Annu. Rev. Mater. Res., 38: 425443.

[20]. Marshall, D. B., Cox, B. N., and Sudre, O. H., (2017) Integral textile structure for 3-D CMC turbine airfoils, US Patent 9,664,053.

[21]. Quinn, J., McIlhagger, R., and McIlhagger, A., (2003) A modified system for design and analysis of 3d woven preforms, Compos. Part A Appl., 34: 503–509.

[22]. Hartranft, D., Pravizi-Majidi, A., and Chou, T.-W., (1995) Modeling and characterization of through-the-thickness properties of 3D woven composites, in: NASA, Langley Research Center Mechanics of Textile Composites Conference.

[23]. Hill, B., McIlhagger, R., (1997) The development and appraisal of 3d fully integrated woven structures for textile reinforced composites, Polym. Polym. Compos., 5: 49–55.

[24]. Pelegri, A. A., and Kedlaya, D. N., (2008) Design of composites using a generic unit cell model coupled with a hybrid genetic algorithm, Compos. Part A Appl. 39: 1433–1443.

[25]. Zeng, X., Long, A. C., Ashcroft, I., and Potluri, P., (2015) Fibre architecture design of 3D woven composite with genetic algorithms: a unit cell based optimisation framework and performance assessment, 20th International Conference on Composite Materials, Copenhagen.

[26]. Fu, X., Ricci, S., and Bisagni, C., (2015) Minimum-weight design for three dimensional woven composite stiffened panels using neural networks and genetic algorithms, Compos. Struct. 134: 708–715.

[27]. Wang, Q., Yang, X., Zhao, H., Zhang, X., Cao, G., and Ren, M., (2021) Microscopic residual stresses analysis and multiobjective optimization for 3D woven composites, Compos. Part A Appl., 144: 106310.

[28]. Verpoest, I. and Lomov, S. V., (2005) Virtual textile composites software wisetex: Integration with micro-mechanical, permeability and structural analysis, Compos Sci Technol, 65: 2563–2574.

[29]. Lin, H., Brown, L. P., and Long, A. C., (2011) Modelling and simulating textile structures using TexGen, in: Advanced Materials Research, 331:4 –47.

[30]. Labanieh, A. R., Legrand, X., Koncar, V., and Soulat, D., (2013) Novel optimization method to estimate the geometrical properties of a multiaxial 3D woven preform, J REINF PLAST COMP, 32: 700–712.

[31]. Spackman, G., Brown, L., and Jones, I., (2018) Development of methods for optimisation of complex 3D weave geometries, in: IOP Conference Series: Materials Science and Engineering, volume 406, IOP Publishing, p. 012029.

[32]. Plaka, E., Jones, S., Bednarcyk, B. A., Pineda, E. J., Li, R., and Maiaru, M., (2022) Application of a rapid design tool to a 3D woven structural joint, in: AIAA SCITECH Forum, 2022, p. 1009.

[33]. Ha, S. and Guest, J. K., (2016) Topology optimization of 3d woven micro-lattices using a projection-based ground structure approach, in: 17th AIAA/ISSMO Multidisciplinary Analysis and Optimization Conference, p. 3214.

[34]. Morioka, K., Ohtake, Y., Suzuki, H., Nagai, Y., Hishida, H., Inagaki, K., Nakamura, T., and Watanabe, F., (2016). 3D woven composite design using a flattening simulation, CAD, 81: 24-38.

[35]. Fu, X., Ricci, S., Bisagni, C., (2017) Multi-scale analysis and optimisation of three-dimensional woven composite structures combining response surface method and genetic algorithms, CEAS Aeronaut. J., 8: 129–141.

[36]. Yan, S., Zeng, X., and Long, A., (2019) Meso-scale modelling of 3d woven composite t-joints with weave variations, Compos Sci Technol, 171: 171–179.

[37]. Daynes, S., Feih, S., Lu, W. F., and Wei, J. (2017). Optimisation of functionally graded lattice structures using isostatic lines. Mat. & Des., 127: 215-223.

[38]. Boyle, C., Kim, I. Y., (2011) Three-dimensional micro-level computational study of wolff's law via

trabecular bone remodeling in the human proximal femur using design space topology optimization, J. Biomech., 44: 935–942.

[39]. Wolff, J. (1986) The Law of Bone Remodeling. Berlin, Springer.